

Complex photonic band structure and effective plasma frequency of a two-dimensional array of metal rods

S. Brand, R. A. Abram, and M. A. Kaliteevski

Department of Physics, Rochester Building, Durham University, Durham DH1 3LE, United Kingdom

(Received 3 July 2006; revised manuscript received 11 October 2006; published 3 January 2007)

A number of simple analytic theories have been proposed to define an effective plasma frequency in two-dimensional (2D) periodic systems containing metallic elements such as an array of metal rods in a simple square lattice. Such metallic structures are considered using a frequency-dependent plane-wave complex band structure approach. Detailed results are presented for the pass and stop bands for a range of rod diameters. In addition, the value of the effective plasma frequency is extracted and compared with the predictions of existing analytic models. For the structures considered the effective plasma frequency is in the THz regime.

DOI: [10.1103/PhysRevB.75.035102](https://doi.org/10.1103/PhysRevB.75.035102)

PACS number(s): 78.20.Bh, 42.70.Qs, 41.20.-q, 42.25.Bs

I. INTRODUCTION

Some time ago Pendry *et al.*^{1,2} considered the problem of the plasma frequency of an array of thin metallic wires, which is a structure whose low frequency response can be characterized in terms of an effective plasma frequency, below which propagating electromagnetic modes do not occur. In their case the theory was specifically designed to deal with very thin wires with an effective plasma frequency shifted into the GHz range from the bulk metal value $\sim 10^{15}$ Hz. Since then a number of alternative simple analytic theories have been proposed in order to deal with this problem.³⁻⁵ In the current work we apply a frequency dependent, plane-wave based, complex photonic band structure approach to the calculation of the effective plasma frequency for a series of structures consisting of an array of circular metal rods in a two-dimensional (2D) square lattice. The plane-wave approach is potentially applicable to a variety of situations in which the permittivity depends on frequency. There has been considerable controversy concerning the results to be expected in the case of much lower frequencies and rather larger lattice spacings where the skin depth and rod diameter are comparable (see for example Markos and Soukoulis⁶ and references therein). However, in our calculations, we are concerned with the case where the skin depth is significantly smaller than the rod diameter, and therefore some of the problems encountered at lower frequencies do not apply. The details of the theory are described in Sec. II with the results presented in Sec. III. Comparison with existing analytic theories for the effective plasma frequency are found in Sec. IV and conclusions in Sec. V.

II. THEORY

The theory described follows a similar formulation to that of our earlier work concerning complex electronic band structure,⁷ and recent complex photonic band structure studies of equifrequency surfaces for superprism applications⁸ carried out within our group. The approach is similar to, but different in some details to that described by Gu *et al.*⁹ We begin by assuming a system with frequency-independent background relative permittivity ϵ_b into which we introduce a 2D periodic array of rods of arbitrary cross section aligned

parallel to the z direction, as shown in Fig. 1. The relative permittivity within the rods is taken to be of the general frequency-dependent form $\epsilon(\omega)$ which may have real and imaginary components that completely characterize the response of the rods. For completeness we consider the situations in which the electric field is polarized either parallel (TM) or perpendicular (TE) to the rods although it is the former case with which we are primarily concerned. In what follows we consider only nonmagnetic materials for which the permeability is μ_0 .

A. TM polarization: E -field polarized in z direction, parallel to rod axis

We take

$$\underline{E}(\underline{r}, t) = \underline{E}(\underline{\rho}, t) = \begin{pmatrix} 0 \\ 0 \\ E_z(\underline{\rho}) \end{pmatrix} e^{-i\omega t},$$

$$\underline{H}(\underline{r}, t) = \underline{H}(\underline{\rho}, t) = \begin{pmatrix} H_x(\underline{\rho}) \\ H_y(\underline{\rho}) \\ 0 \end{pmatrix} e^{-i\omega t},$$

where \underline{r} is the position vector, $\underline{\rho} = (x, y)$ is the 2D position vector and the electric field in the z direction can be expressed as a Fourier series expansion in terms of the reciprocal lattice vectors \underline{g}

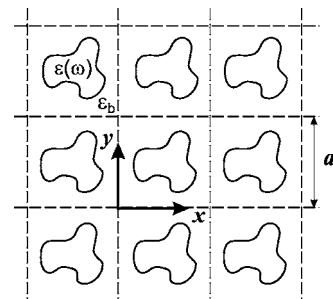


FIG. 1. An array of arbitrary shaped rods in a square lattice. Within the rods the frequency-dependent permittivity $\epsilon(\underline{\rho}) = \epsilon(\omega)$ and elsewhere $\epsilon(\underline{\rho}) = \epsilon_b$, a constant background value.

$$E_z(\underline{\rho}) = \sum_{\underline{g}} E_{\underline{g}} e^{i(\underline{k}+\underline{g})\cdot\underline{\rho}}. \quad (1)$$

\underline{k} is a wave vector perpendicular to the z direction. We then have, from Maxwell's equations

$$\nabla \times \underline{E}(\underline{\rho}, t) = i\omega\mu_0 \underline{H}(\underline{\rho}, t), \quad \nabla \times \underline{H}(\underline{\rho}, t) = -i\omega\varepsilon_0 \varepsilon(\underline{\rho}) \underline{E}(\underline{\rho}, t)$$

and hence

$$\nabla \times \nabla \times \underline{E}(\underline{\rho}, t) = i\omega\mu_0 \nabla \times \underline{H}(\underline{\rho}, t) = i\omega\mu_0 [-i\omega\varepsilon_0 \varepsilon(\underline{\rho}) \underline{E}(\underline{\rho}, t)] = \frac{\omega^2}{c^2} \varepsilon(\underline{\rho}) \underline{E}(\underline{\rho}, t).$$

This equation has only a z component and so, dropping the common $e^{-i\omega t}$ factor, we have

$$\sum_{\underline{g}} E_{\underline{g}} (\underline{k} + \underline{g})^2 e^{i(\underline{k}+\underline{g})\cdot\underline{\rho}} = \frac{\omega^2}{c^2} \varepsilon(\underline{\rho}) \sum_{\underline{g}} E_{\underline{g}} e^{i(\underline{k}+\underline{g})\cdot\underline{\rho}}, \quad (2)$$

where we have made use of (1) to obtain the expression for $\nabla \times \nabla \times \underline{E}(\underline{\rho}, t)$ on the left-hand side of (2).

We now write the spatial dependence of the permittivity $\varepsilon(\underline{\rho})$ in the form

$$\varepsilon(\underline{\rho}) = \varepsilon_b + [\varepsilon(\omega) - \varepsilon_b] S(\underline{\rho}),$$

where

$$S(\underline{\rho}) = 1 \quad \text{within the } \omega\text{-dependent region,}$$

$$S(\underline{\rho}) = 0 \quad \text{elsewhere.}$$

We then employ a Fourier series expansion $S(\underline{\rho}) = \sum_{\underline{g}'} S_{\underline{g}'} e^{i\underline{g}'\cdot\underline{\rho}}$ so that (2) can be rewritten in the form

$$\sum_{\underline{g}} E_{\underline{g}} (\underline{k} + \underline{g})^2 e^{i(\underline{k}+\underline{g})\cdot\underline{\rho}} = \frac{\omega^2 \varepsilon_b}{c^2} \sum_{\underline{g}} E_{\underline{g}} e^{i(\underline{k}+\underline{g})\cdot\underline{\rho}} + F_1(\omega) \sum_{\underline{g}', \underline{g}} S_{\underline{g}'} E_{\underline{g}} e^{i(\underline{k}+\underline{g}+\underline{g}')\cdot\underline{\rho}}, \quad (3)$$

where, for convenience, we have defined $F_1(\omega) = \frac{\omega^2}{c^2} [\varepsilon(\omega) - \varepsilon_b]$.

Multiplying (3) by $e^{-i(\underline{k}+\underline{G})\cdot\underline{\rho}}$, where \underline{G} is any reciprocal lattice vector, and integrating over a unit cell we obtain a set of equations

$$E_{\underline{G}} \left[(\underline{k} + \underline{G})^2 - \frac{\omega^2 \varepsilon_b}{c^2} \right] = F_1(\omega) \sum_{\underline{g}} S_{\underline{G}-\underline{g}} E_{\underline{g}}. \quad (4)$$

In matrix form these equations can be combined to give $M\underline{E} = F_1(\omega) S\underline{E}$ where M is a diagonal matrix with elements given by

$$M_{\underline{G}, \underline{G}} = (\underline{k} + \underline{G})^2 - \frac{\omega^2 \varepsilon_b}{c^2},$$

the matrix S has elements given by the Fourier components $S_{\underline{G}, \underline{g}} = S_{\underline{G}-\underline{g}}$ and the components of the eigenvector \underline{E} are the E -field expansion coefficients $E_{\underline{g}}$. If we then take $\underline{k} = k\hat{u}$ where \hat{u} is a two-dimensional unit vector in the x - y plane

defining the wave vector direction, (4) can be rewritten in the form

$$k^2 I \underline{E} + k A \underline{E} + B \underline{E} = C \underline{E},$$

$$\text{or } k^2 I \underline{E} + k A \underline{E} = (C - B) \underline{E} = D \underline{E}, \quad (5)$$

where

I is the identity matrix,

A only has diagonal elements given by $A_{\underline{G}, \underline{G}} = 2\underline{G} \cdot \hat{u}$,

B only has diagonal elements given by $B_{\underline{G}, \underline{G}} = G^2 - \frac{\omega^2}{c^2} \varepsilon_b$,

C has the elements

$$C_{\underline{G}, \underline{g}} = F_1(\omega) S_{\underline{G}, \underline{g}}.$$

In a standard plane-wave photonic band structure calculation as employed by Plihal and Maradudin,¹⁰ for example, $1/\varepsilon(\underline{\rho})$ is expanded as a Fourier series and the eigenvalue equation is such that ω^2 can be found for a given \underline{k} . However, here (5) is reformulated as a matrix of order $2n \times 2n$, where n is the number of plane waves employed in the expansion of the E field to give the general complex eigenvalue equation

$$\begin{pmatrix} 0 & I \\ D & -A \end{pmatrix} \begin{pmatrix} \underline{E} \\ k\underline{E} \end{pmatrix} = k \begin{pmatrix} \underline{E} \\ k\underline{E} \end{pmatrix} \quad (6)$$

from which we may obtain the general complex wave vectors k for the direction \hat{u} for a given fixed ω as long as $\varepsilon(\omega)$ is known. We can then perform a frequency scan to obtain the complex photonic band structure. The electric field can also be obtained from the eigenvectors of Eq. (6) (and then the magnetic field from the appropriate Maxwell equation) but we do not give any results for the field profiles in this work.

B. TE polarization: H -field polarized in z direction, parallel to rod axis

We take

$$\underline{H}(\underline{r}, t) = \underline{H}(\underline{\rho}, t) = \begin{pmatrix} 0 \\ 0 \\ H_z(\underline{\rho}) \end{pmatrix} e^{-i\omega t},$$

$$\underline{E}(\underline{r}, t) = \underline{E}(\underline{\rho}, t) = \begin{pmatrix} E_x(\underline{\rho}) \\ E_y(\underline{\rho}) \\ 0 \end{pmatrix} e^{-i\omega t},$$

where

$$H_z(\underline{\rho}) = \sum_{\underline{g}} H_{\underline{g}} e^{i(\underline{k}+\underline{g})\cdot\underline{\rho}}.$$

In this case we employ Maxwell's equations in the form

$$\nabla \times \underline{E}(\underline{\rho}, t) = i\omega\mu_0 \underline{H}(\underline{\rho}, t)$$

and

$$\frac{1}{\varepsilon(\underline{\rho})} \nabla \times \underline{H}(\underline{\rho}, t) = -i\omega\varepsilon_0 \underline{E}(\underline{\rho}, t)$$

and combining them gives

$$\nabla \times \left[\frac{1}{\varepsilon(\underline{\rho})} \nabla \times \underline{H}(\underline{\rho}, t) \right] = -i\omega\varepsilon_0 \nabla \times \underline{E}(\underline{\rho}, t) = -i\omega\varepsilon_0 [i\omega\mu_0 \underline{H}(\underline{\rho}, t)] = \frac{\omega^2}{c^2} \underline{H}(\underline{\rho}, t). \quad (7)$$

The reciprocal of the permittivity can be written as

$$\frac{1}{\varepsilon(\underline{\rho})} = \frac{1}{\varepsilon_b} - \frac{[\varepsilon(\omega) - \varepsilon_b]}{\varepsilon_b \varepsilon(\omega)}. S(\underline{\rho}) = \frac{1}{\varepsilon_b} [1 - F_2(\omega) S(\underline{\rho})], \quad (8)$$

where

$$F_2(\omega) = \frac{\varepsilon(\omega) - \varepsilon_b}{\varepsilon(\omega)}.$$

[Note that for the cases considered in Sec. III, $F_2(\omega) \approx 1$ but we do not make use of this approximation.]

Substitution of (8) in (7) leads to

$$\nabla \times \{ [1 - F_2(\omega) S(\underline{\rho})] \nabla \times \underline{H}(\underline{\rho}, t) \} = \frac{\omega^2 \varepsilon_b}{c^2} \underline{H}(\underline{\rho}, t). \quad (9)$$

We then proceed in a similar manner to before by inserting the plane wave expansions for $S(\underline{\rho})$ and $H_z(\underline{\rho})$ in (9) to give

$$\sum_{\underline{g}} H_{\underline{g}} (\underline{k} + \underline{g})^2 e^{i(\underline{k}+\underline{g})\cdot\underline{\rho}} - F_2(\omega) \sum_{\substack{\underline{g}, \underline{g}' \\ \underline{g}, \underline{g}'}} S_{\underline{g}, \underline{g}'} H_{\underline{g}} (\underline{k} + \underline{g}) \cdot (\underline{k} + \underline{g} + \underline{g}') e^{i(\underline{k}+\underline{g}+\underline{g}')\cdot\underline{\rho}} = \frac{\omega^2 \varepsilon_b}{c^2} \sum_{\underline{g}} H_{\underline{g}} e^{i(\underline{k}+\underline{g})\cdot\underline{\rho}}. \quad (10)$$

Multiplying (10) by $e^{-i(\underline{k}+\underline{g})\cdot\underline{\rho}}$, and integrating over a unit cell gives, after some rearrangement

$$H_{\underline{G}} (\underline{k} + \underline{G})^2 - \frac{\omega^2 \varepsilon_b}{c^2} H_{\underline{G}} = F_2(\omega) \sum_{\underline{g}} S_{\underline{G}-\underline{g}} (\underline{k} + \underline{G}) \cdot (\underline{k} + \underline{g}) H_{\underline{g}}. \quad (11)$$

We can write (11) in matrix form as

$$M \underline{H} = k^2 I \underline{H} + k A \underline{H} + B \underline{H} = F_2(\omega) S' \underline{H}, \quad (12)$$

where M , A , and B are the same matrices as defined in the case of TM polarization, \underline{H} is a vector with the $H_{\underline{g}}$ expansion coefficients for components, and the elements of the matrix S' are given by

$$S'_{\underline{G}, \underline{g}} = (\underline{k} + \underline{G}) \cdot (\underline{k} + \underline{g}) S_{\underline{G}-\underline{g}} = [k^2 + k \underline{\hat{u}} \cdot (\underline{G} + \underline{g}) + \underline{G} \cdot \underline{g}] S_{\underline{G}-\underline{g}}.$$

The right-hand side of Eq. (12) can be rewritten as

$$F_2(\omega) S' \underline{H} = (k^2 P + k Q + R) \underline{H},$$

where

$$P \text{ has the elements given by } P_{\underline{G}, \underline{g}} = F_2(\omega) S_{\underline{G}-\underline{g}},$$

$$Q \text{ has the elements given by } Q_{\underline{G}, \underline{g}} = F_2(\omega) S_{\underline{G}-\underline{g}} \underline{\hat{u}} \cdot (\underline{G} + \underline{g}),$$

$$R \text{ has the elements given by } R_{\underline{G}, \underline{g}} = F_2(\omega) S_{\underline{G}-\underline{g}} \underline{G} \cdot \underline{g}.$$

With these definitions we can rewrite Eq. (12) in the form

$$M \underline{H} = k^2 I \underline{H} + k A \underline{H} + B \underline{H} = k^2 P \underline{H} + k Q \underline{H} + R \underline{H}$$

or

$$k^2 (I - P) \underline{H} + k (A - Q) \underline{H} = (R - B) \underline{H}. \quad (13)$$

Multiplying Eq. (13) by the inverse matrix $(I - P)^{-1}$ gives

$$k^2 I \underline{H} + k A' \underline{H} = D' \underline{H}, \quad (14)$$

where we define $A' = (I - P)^{-1} (A - Q)$, $D' = (I - P)^{-1} (R - B)$.

We then observe that Eq. (14) has identical structure to Eq. (5) as it can be rewritten in the form

$$\begin{pmatrix} 0 & I \\ D' & -A' \end{pmatrix} \begin{pmatrix} \underline{H} \\ k \underline{H} \end{pmatrix} = k \begin{pmatrix} \underline{H} \\ k \underline{H} \end{pmatrix}. \quad (15)$$

If $\varepsilon(\omega)$ is known, we may again obtain the general complex wave vectors k for the direction $\underline{\hat{u}}$ for a given ω and then scan through frequency dependent to map out the associated complex photonic band structure.

It is noted that alternative plane-wave complex photonic band structure approaches have been described by Treacy¹¹ and Shi *et al.*¹² [these authors employ a different expansion of $\varepsilon(\underline{\rho})$ or $1/\varepsilon(\underline{\rho})$ which leads to a somewhat different formulation] and complex band structure results have also been given by Pendry *et al.*² for a thin 2D thin wire array. Both the

approaches of Gu *et al.*⁹ and Pearce *et al.*¹³ can also deal with general $\varepsilon(\omega)$ including imaginary components but in all of the above cases^{9,11–13} a frequency-dependent Fourier series expansion is employed leading to somewhat different formulations from that employed in our work.

III. RESULTS

We now apply the theory described in Sec. II to the situation in which we have a 2D square array of circular metal rods of diameter $2r$ and lattice constant $a=200\ \mu\text{m}$. A set of structures is considered with a range of rod diameters from 10–120 μm . The lattice period of 200 μm is similar, although somewhat smaller, to that employed in the experimental work of Pimenov and Loidl¹⁴ who considered 2D arrays of copper and steel wires. The values of r and the period have been chosen to ensure an effective plasma frequency in the THz regime. This is a regime which is accessible to fabrication employing standard lithographic and sputtering techniques.

For the purposes of the calculation we take the background relative permittivity $\varepsilon_b=1$ as appropriate for air and for the circular rods we take

$$\varepsilon(\omega) = 1 - \frac{\omega_p^2}{\omega(\omega + i\omega_c)}, \quad (16)$$

where ω_p is the bulk metal plasma frequency and ω_c is a constant describing the absorption. In this case we employ the values of Ordal *et al.*¹⁵ for gold: $\omega_p=2\pi\times 2.175\times 10^{15}\ \text{s}^{-1}$, $\omega_c=2\pi\times 6.5\times 10^{12}\ \text{s}^{-1}$.

To begin, we present typical complex photonic band structure results for the TM case, both excluding and including the absorption term in Eq. (16). These are shown in Figs. 2 and 3, respectively. (In the figures it should be noted that there is no special significance to the sign of the real and imaginary k components: the k values come in pairs with positive and negative imaginary components corresponding to decay in opposite directions. The sign convention employed here is purely for plotting convenience.) These particular calculations were performed with the wave vector in the [100] direction for midrange 50 micron diameter rods and employed 805 plane waves for the expansion of the E field. In the plots, k is given in units of $2\pi/a$ and the results in Fig. 2 indicate that the main purely imaginary solutions are heavily attenuated; indeed $\text{Im}(k)\approx 0.15\times 2\pi/a$, corresponding to the center of the general complex solution centred at about 1 THz implies a decay length for E of about 1 lattice constant. Note that for these general complex wave vectors, the real part of k is attached to the edge of the Brillouin zone and solutions with $\text{Re}(k)=\pm 0.5\times 2\pi/a$ are equivalent as they differ by a reciprocal lattice vector. In the range displayed, the results indicate that there are two bands in which propagation is possible between about 0.67 \rightarrow 0.84 THz and 1.16 \rightarrow 1.53 THz: in these regions the value of k is purely real. Note that when solutions are purely real or purely imaginary, as in this case, there is no energy dissipation and we would conclude that any electromagnetic (EM) wave impinging on a semi-infinite system would be either

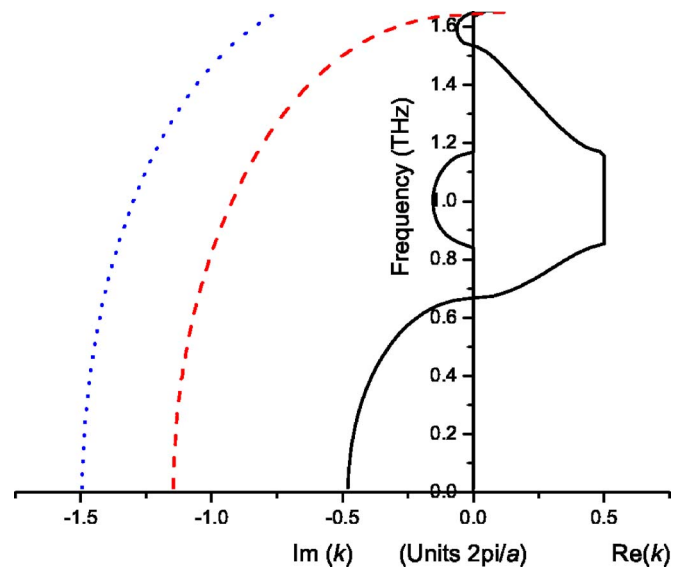


FIG. 2. (Color online) Complex photonic band structure in the [100] direction for 50 micron diameter rods in a 200 micron period square lattice. The absorption term is omitted in this calculation. Dotted and dashed lines relate to purely imaginary k values and the solid lines relate to purely imaginary, purely real, or their connected general complex solutions.

100% reflected, if the imaginary component of k is nonzero, or may propagate to some extent through the structure, depending on the reflection coefficient at the surface, if k is purely real.

We now consider the effect of the inclusion of the absorption term ω_c as demonstrated by the results in Fig. 3. In this case all k are of general complex form, and hence a degree of energy dissipation is always present, as we would expect for a metal, although the respective real or imaginary components may be very small. We see that there is no qualitative

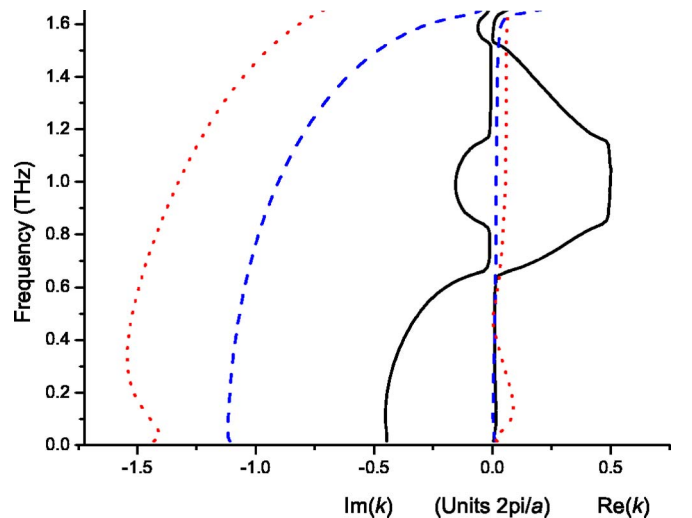


FIG. 3. (Color online) Complex photonic band structure in the [100] direction for 50 micron diameter rods in a 200 micron period square lattice. The absorption term is included in this calculation. In this case all solutions are general complex (with solid, dotted and dashed real and imaginary solutions paired as shown).

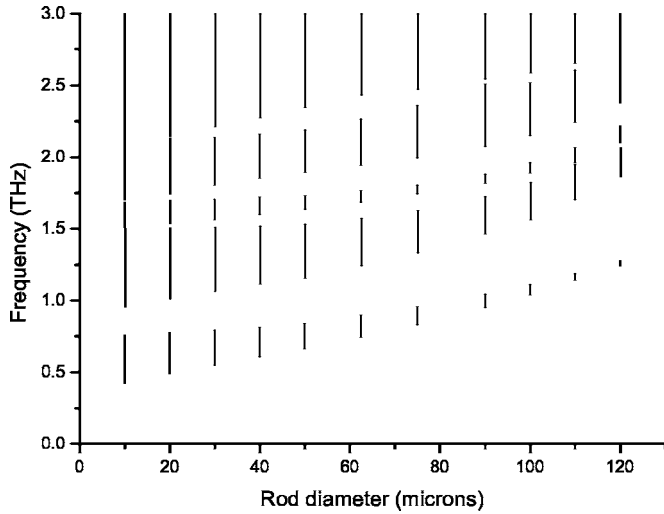


FIG. 4. Evolution of the pass bands (real k regions) as a function of rod diameter for 200 μm period structures.

change in the overall band structure except in the case of the most heavily attenuated solution which displays a significant dip in the imaginary component and a corresponding significant peak in its real component. This region indicates the existence of both positive, negative, and infinite group velocities, although the interpretation of this is somewhat open to question since we have energy dissipation and such heavily attenuated solutions. Although it is clearly more problematic to define the band edge in this case, the relatively small value of the imaginary component of k , corresponding to the general area of our original pass bands, indicates that for any finite structure significant propagation may still be possible in the same ranges as indicated by our original calculations without the ω_c term. In view of this we shall for the moment follow the widespread convention of neglecting the ω_c term, and in what follows define the band edges as the frequencies at which k changes from purely imaginary to purely real or vice versa.

With the neglect of ω_c , we show in Fig. 4 the evolution of the pass bands (purely real k regions) as a function of rod diameter. The positions of the band edges have been established using 877 plane waves, which our calculations indicate give convergence to about 2% for the lowest frequency solutions in which we are primarily interested. A significant feature of the first two bands displayed is that, despite an order of magnitude change in rod diameter, and a much larger change in fill factor, the change in position of the bands is relatively modest, especially in the case of band 2, the center of which only shifts from about 1.2 THz to 1.7 THz as rod diameter is increased from 10 to 100 μm . The center of band 1 shifts by a factor of about 2 over the same range. In addition we note a consistent narrowing of both bands with increasing diameter. We note that the existence of such pass and stop band regions, which can be modified in width and position by varying period and rod diameter, is potentially useful in THz filter applications. Experiments are currently being conducted by other workers in Durham in an attempt to establish the reliability of our theoretical predictions concerning the detailed form of the

pass and stop bands for the above series of 200 μm period structures.

In principle, to simulate fully the effects of absorption within the metal rods when the absorption term is included, we might expect that it would be necessary to represent the detailed form of the E field within the skin depth region near the surface of the rods. For the frequencies considered the skin depth is a small fraction of a micrometer and it is well beyond the capabilities of our calculations to represent the E field profile accurately with the number of plane waves employed. In practice it is clear from our calculations that whereas the convergence of the value of the imaginary component is in fact rather poorer than, for example, the position of the band edges, it can nevertheless still provide some information concerning at least the minimum decay length within the structure [the trend in the value of $\text{Im}(k)$ in the “pass band” regions is to decrease with increasing number of plane waves]. In the case of the 10 μm diameter rods, the indicated E field decay length appears to be in excess of 75 periods and, at least for fairly low diameter rods, the decay length is roughly proportional to rod diameter and hence area. Even for 50 μm diameter rods, the decay length is indicated to be in excess of 15 periods. Tests indicate that the decay lengths are not greatly changed even with a significantly increased value of ω_c , particularly for the second pass band, so we would confidently expect to observe substantial transmission through finite structures. For the large diameter rods, e.g. ≈ 100 μm or similar, the convergence of the imaginary component of k is significantly worse and the losses appear to be rather high, suggesting that the narrower pass bands indicated in the absorption-free calculations may not be achievable in practice.

IV. EFFECTIVE PLASMA FREQUENCY

In addition to the more detailed results concerning the general form of the photonic band structure, we can also make use of the results in Fig. 4 to define an effective plasma frequency, or cut-off frequency, for this series of structures. This is the lowest frequency at which propagation is allowed through the structure when k first becomes purely real with increasing frequency at the bottom of the first pass band. This value is plotted in Fig. 5 as a function of rod diameter. To give an indication of the possible consequences of convergence errors we also display a line in which the calculated values have been reduced by 2%. Some simple analytical expressions for the effective plasma frequency $\nu_{p,eff}$ have previously been given by various authors as listed below: Pendry *et al.*^{1,2}

$$\nu_{p,eff}^2 = \frac{c^2}{2\pi a^2 \ln(a/r)},$$

Sarychev and Shalaev³

$$\nu_{p,eff}^2 = \frac{c^2}{2\pi a^2 [\ln(\sqrt{2}a/r) + \pi/2 - 3]},$$

Maslovski *et al.*⁴

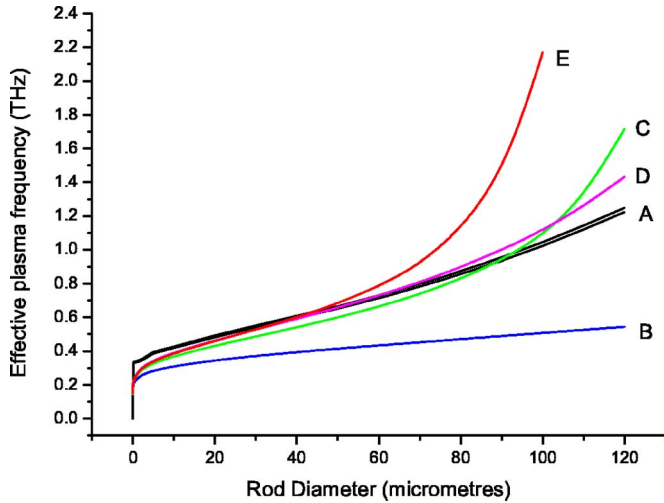


FIG. 5. (Color online) The effective plasma frequency as a function of rod diameter as obtained in the present calculations ((A) a line is also shown with values reduced by 2%) and using the expressions of Pendry *et al.* (B), Sarychev and Shalaev (C), Maslovski (D), and Tretyakov (E).

$$v_{p,eff}^2 = \frac{c^2}{2\pi a^2 \ln[a^2/(4r(a-r))]},$$

Tretyakov⁵

$$v_{p,eff}^2 = \frac{c^2}{2\pi a^2 [\ln(a/(2\pi r)) + 0.5275]},$$

and these plots are also shown in the figure.

We note that such simplified analytic models are not able to account for the detailed band structure effects resulting from the electromagnetic field distribution within the system and their range of validity may be unclear. In the case of Pendry *et al.*² the theoretical model was designed to apply to thin wire structures and the prototype system consisted of a 2 μm diameter wire in a 5 mm period square lattice. Similarly, the Tretyakov expression is stated as being valid with $r < a/100$. In the case of the large diameter rods considered in the present work the band structure effects cannot be discounted, the thin wire assumptions clearly do not apply, and hence our calculations represent an important independent indicator of the range of validity of these simpler models. In comparing our results with those of the Pendry *et al.* model we might initially conclude that their model is rather poor. However, given that the model was originally devised explicitly for the case of very thin wires it may be more appropriate to conclude that it is surprisingly good under the circumstances. The Tretyakov results are in reasonable agreement for the smaller rod diameters (although still at much greater diameters than the suggested range of validity) but become much higher than our results for larger diameters. The results of both Sarychev and Shalaev and Maslovski are in quite good agreement with the present work, although on balance those of Maslovski, appear to be superior, particularly at the higher rod diameters. We note that the plane-wave calculations cannot be expected to perform well at very small rod

diameters, and indeed below about 10 μm they appear somewhat erratic due to the limited number of plane waves employed in the calculation, which is insufficient to define the structure reliably in such cases. Although the results themselves are not reliable in the small diameter regime, we note that at very small diameters the plane-wave calculations give numerical results which are consistent with a simple effective medium model with the results agreeing almost exactly with the expression $v_{p,eff}^2 = \frac{f\omega_p^2}{4\pi^2} = f v_p^2$ where f is the metallic fill factor.

Without the ω_c absorption term the calculations involve no energy dissipation and the plane-wave calculation in effect attempts to exclude the E field from the metallic regions within the limitations imposed by the finite number of plane waves used. In this case the convergence of the results appears to be good, as already discussed. The method also gives results in agreement with the work of Kuzmiak *et al.*¹⁶ when applied to structures in which the effective plasma frequency is much closer to the bulk value i.e. in the regime where the lattice constant is near the bulk plasma frequency wavelength in free space. The method of Kuzmiak *et al.* is essentially a modified standard plane-wave approach designed to take advantage of the specific form of the permittivity expression $\epsilon(\omega) = 1 - \omega_p^2/\omega^2$, but does not work in more general frequency-dependent cases. Due to the relatively low value of the effective plasma frequency in our structures, which is well removed from the bulk value, we have also performed standard plane wave photonic band structure calculations employing a large and constant negative value for $\epsilon(\omega)$, as this may be considered likely to give reasonable results in this regime. However, we find that although it is possible to identify bands of the same form as those in the current calculations, the convergence is significantly worse and we believe this more than justifies the use of the $2n \times 2n$ matrices required for the complex band structure calculations. Given that in our calculations the fields are primarily confined to the “background” regions with very little penetration into the metal rods, the explicit separation of $\epsilon(\rho)$ or $1/\epsilon(\rho)$ into background plus rod regions, rather than using a single Fourier expansion can be expected to have been an aid to convergence: this is unlike the other formulations^{9,11–13} which do not employ such a separation and thus require a completely different Fourier expansion at each ω . We simply have the same Fourier expansion but a different $F_1(\omega)$ or $F_2(\omega)$.

As an additional test of the plane-wave approach, we have carried out calculations to obtain results for the experimental structures studied by Pimenov and Loidl¹⁴ and observe that the positions of the calculated bands appear to be entirely consistent with their transmission results.

In practice, the concept of an effective plasma frequency in such periodic structures applies only to the TM polarization for which we have presented detailed results. In this case the system basically behaves as a standard waveguide structure with the results controlled by the boundary condition at the surface of the rods which effectively means that $E \rightarrow 0$ within the rods very close to the surface. The detailed behavior within the skin depth region is generally not important for the general form of the photonic band structure. For the TE

polarization the requirement that E is perpendicular to the axis of the rods leads to results rather similar to those seen for a standard dielectric structure, as observed by Sigalas *et al.*¹⁷ We find that the TE polarization photonic bands are consistent with the predictions of Kuzmiak *et al.* and also the experimental and theoretical FDTD results of Sigalas *et al.*, and in this case show little structure apart from some narrow band gaps. In particular, there is no effective plasma or cut-off frequency for this polarization.

V. CONCLUSIONS

We have employed a theoretical formalism for computing the plane-wave complex photonic band structure of a system containing components having a general frequency-dependent permittivity. In the regime considered this has significantly better convergence properties than a standard plane-wave calculation employing a large constant negative value for ϵ , which is an otherwise fairly reasonable approach to take. In applying the formalism to the calculation of the photonic band structure of a square array of metal rods, we obtain a well-converged band structure displaying a characteristic series of pass bands and a cut-off or effective plasma

frequency in the THz region in the case of 200 μm period structures. Experimental work by others in Durham is currently underway in an attempt to verify our theoretical predictions for the detailed band structures. Although we nominally considered gold rods in our calculations, the results are expected to be essentially identical for any metallic rod structure with similar rod diameter and period and typical bulk plasma frequency. The THz region considered is sufficiently far from the bulk plasma frequency that the precise value of ω_p is not important in determining the detailed numerical results. In comparing the results for our calculated effective plasma frequency with those of simpler analytic models which do not account for the detailed band structure effects, and therefore whose range of validity is uncertain, we conclude that the model of Maslovski⁴ appears to be most consistent with our results over the range considered. We anticipate that the THz region pass bands displayed in our results may be utilisable in THz filter applications.

ACKNOWLEDGMENTS

M.A.K. acknowledges the financial assistance of EPSRC via Grant No EP/C534263.

¹J. B. Pendry, A. J. Holden, W. J. Stewart, and I. Youngs, *Phys. Rev. Lett.* **76**, 4773 (1996).

²J. B. Pendry, A. J. Holden, D. J. Robbins, and W. J. Stewart, *J. Phys.: Condens. Matter* **10**, 4785 (1998).

³A. K. Sarychev and V. M. Shalaev, cond-mat/0103145 (unpublished).

⁴S. I. Maslovski, S. A. Tretyakov, and P. A. Belov, *Microwave Opt. Technol. Lett.* **35**, 47 (2002).

⁵S. Tretyakov, *Analytical Modeling*, in *Applied Electromagnetics* (Artech House Publishing, 2004).

⁶P. Markos and C. M. Soukoulis, *Opt. Lett.* **28**, 846 (2003).

⁷S. Brand and D. T. Hughes, *Semicond. Sci. Technol.* **2**, 607 (1987).

⁸A. A. Reeves, Ph.D. thesis, *Theoretical Studies of One-Dimensional and Two-Dimensional Photonic Structures*, University of Durham, 2004.

⁹B.-Y. Gu, L.-M. Zhao, and Y.-C. Hsue, *Phys. Lett. A* **355**, 134 (2006).

¹⁰M. Plihal and A. A. Maradudin, *Phys. Rev. B* **44**, 8565 (1991).

¹¹M. M. J. Treacy, *Phys. Rev. B* **66**, 195105 (2002).

¹²S. Shi, C. Chen, and D. W. Prather, *Appl. Phys. Lett.* **86**, 043104 (2005).

¹³G. J. Pearce, T. D. Hedley, and D. M. Bird, *Phys. Rev. B* **71**, 195108 (2005).

¹⁴A. Pimenov and A. Loidl, *Phys. Rev. Lett.* **96**, 063903 (2006).

¹⁵M. A. Ordal, L. L. Long, R. J. Bell, R. R. Bell, R. W. Alexander, Jr., and C. A. Ward, *Appl. Opt.* **22**, 1099 (1983).

¹⁶V. Kuzmiak, A. A. Maradudin, and F. Pincemin, *Phys. Rev. B* **50**, 16835 (1994).

¹⁷M. M. Sigalas, C. T. Chan, K. M. Ho, and C. M. Soukoulis, *Phys. Rev. B* **52**, 11744 (1995).